High-Efficient Energy Storage into Eco-Compatible Electrode Materials via Co-intercalation Li^+/Mg^{2+} reactions

Sv. Veleva[1], Sv. Ivanova[2], P. Polrolniczak[3], K. Wasinski[3], D. Nihtyanova[2], R. Stoyanova[2], A. Stoyanova[1]

[1] Institute of Electrochemistry and Energy Systems, Bulgarian Academy of Sciences, Sofia 1113, Bulgaria
[2] Institute of General and Inorganic Chemistry, Bulgarian Academy of Sciences, Sofia 1113, Bulgaria
[3] Institute of Non-Ferrous Metals, Division in Poznań, Central Laboratory of Batteries and Cells, 61-362 Poznań, Poland

Abstract

The storage of energy by means of reversible intercalation of two-valent magnesium ions represents, nowadays, the shortest route to doubling the energy density of conventional lithium ion batteries. Contrary to the intercalation of monovalent lithium ions, the intercalation of Mg^{2+} is kinetically limited process. Herein we demonstrate a new approach for improvement of the kinetic of Mg^{2+} intercalation, which is based on dual intercalation of Li^+- and Mg^{2+} ions with synergic effect. The concept is proven on the basis of two eco-compatible oxides that are highly-efficient for Mg^{2+} storage: magnesium manganese spinel, $MgMn_2O_4$, and monoclinic lithium titanate, Li_2TiO_3. These two types of oxides are selected since they exhibit high and low potentials of ion intercalation due to the redox couples $Mn^{2,3+}/Mn^{3,4+}$ and Ti^{3+}/Ti^{4+}, respectively. The intercalation properties of $MgMn_2O_4$ and Li_2TiO_3 are examined in model cells versus metallic Li anode. The Li^+ and Mg^{2+} intercalation is directed by the kind of the used electrolyte: lithium electrolyte consisting of 1M $LiPF_6$ solution in EC:DMC and magnesium electrolyte – 0.5 $Mg(TFSI)_2$ solution in diglyme. The mechanism of Li^+ and Mg^{2+} co-intercalation is accessed by *ex-situ* X-ray diffraction (XRD) and high-resolution transmission electron microscopy (HR-TEM). The knowledge on the co-intercalation of Li^+ and Mg^{2+} is of significance to construct hybrid Li-Mg-ion cell by combining $MgMn_2O_4$ with Li_2TiO_3 oxides as electrodes.

Keywords: post-lithium ion batteries, intercalation, energy saving, lithium titanium oxides

Introduction

Searching for efficient and safe energy storage devices, nowadays magnesium ion batteries are considered as most competitive alternative to well-known lithium ion batteries [1]. Both magnesium and lithium ion batteries operate by the same mechanism of reversible intercalation of Mg^{2+} an Li^+ ions, but the replacement of monovalent Li^+ with divalent Mg^{2+} ions will provoke a doubling of the battery capacity [1].

Magnesium-ion technology is promising for several reasons. First, due to the natural abundance of magnesium in the earth's crust, approximately 104 times that of lithium, its incorporation into electrode materials is inexpensive. Secondly, magnesium is more air stable and has a higher melting point than lithium, making it safer relative to lithium. The divalent nature of magnesium ions also presents a potential advantage in terms of volumetric capacity (3833 mAh/cm^3 for Mg vs. 2046 mAh/cm^3 for Li) [2].

Despite these positive attributes, the development of magnesium-ion technology has not kept pace with that of lithium ion technology. One critical issue impeding progress is the development of a suitable electrolyte which will enable reversible release of Mg^{2+} ions from a magnesium metal anode [3]. Unlike Li^+ ion conducting surface films formed by polar aprotic electrolyte solutions on Li metal electrodes, surface films on magnesium metal often block the transport of Mg^{2+} ions [4].

A second ongoing challenge is the development of electrode materials which have high reversible capacity and adequate operating voltage under appropriate power output conditions. However, there are many obstacles for Mg^{2+} intercalation in electrode materials: slow kinetics and lack of reversibility of the intercalation reaction, which in its turn are a consequence of significant polarizing and structural transformations taking place with the "host" compound in attempt to compensate locally the two charges of Mg^{2+}. Recent work suggests that low Mg^{2+} mobility is caused by both strong ionic interactions as well as redistribution of the divalently charged cations in the host material [5]. Unfortunately, the potential for the Mg ion intercalation/deintercalation reaction of the Chevrel phase is rather low (formal potential of 1,14 V versus Mg). There are very few materials, which show an intercalation reaction with Mg ions at all, for example V_2O_5 and α-MnO_2 [3, 6]. Various other compounds and alloys, have been investigated, such as TiS_2 (layered [7] or spinel [8] structures), MoO_3 [9], RuO_2 [10], $Mo_{2.5+y}VO_{9+\delta}$ [11], and Prussian blue (PB) analogues ($A_xNiFe(CN)_6$, $A_xCuFe(CN)_6$) [12, 13]. Most of these materials showed a discharge voltage below 2 V vs. Mg/Mg^{2+}, except for the PB analogues. Recently, transition metal polyanion compounds received some attention, however those based on iron, manganese and cobalt silicate showed no reversible intercalation reaction [14, 15]. The electrochemical magnesium insertion/deinsertion into/from a potassium nickel hexacyanoferrate ($K_{0.86}Ni[Fe(CN)_6]_{0.954}(H_2O)_{0.766}$, KNF-086) cathode was studied using a 0.5 M $Mg(ClO_4)_2$ organic electrolyte. The cathode exhibited an excellent

electrochemical reversibility with a capacity of 48.3 mAh/g at a 0.2 C rate, and an average discharge voltage of 2.99 V (vs. Mg/Mg^{2+})[16].

These results show the feasibility of a promising high voltage cathode material for magnesium-ion battery, and could highly motivate the search for new cathode materials with a higher capacity and discharge voltage in nonaqueous electrolyte systems. Therefore, the state-of-the art research is mainly devoted to the improvement of the kinetic of Mg^{2+} intercalation by engineering of nano-sized electrodes [1].

Herein we demonstrate a new approach for improvement of the kinetic of Mg^{2+} intercalation, which is based on dual intercalation of Li^+ ions Mg^{2+} ions with synergic effect. The concept is proven on the basis of two eco-compatible oxides that are highly-efficient for Mg^{2+} storage: magnesium manganese spinel with normal and inverse cationic distribution, $MgMn_2O_4$, and monoclinic lithium titanate, Li_2TiO_3. These two types of oxides are selected since they exhibit high and low potentials of ion intercalation due to the redox couples $Mn^{2,3+}/Mn^{3,4+}$ and Ti^{3+}/Ti^{4+}, respectively. The intercalation properties of $MgMn_2O_4$ and Li_2TiO_3 are examined in model cells versus metallic Li anode. The Li^+ and Mg^{2+} intercalation is directed by the kind of the used electrolyte: lithium electrolyte consisting of 1M $LiPF_6$ solution in EC:DMC and magnesium electrolyte – 0.5 $Mg(TFSI)_2$ solution in diglyme. The mechanism of Li^+ and Mg^{2+} co-intercalation is accessed by *ex-situ* X-ray diffraction (XRD) and high-resolution transmission electron microscopy (HR-TEM). The knowledge on the co-intercalation of Li^+ and Mg^{2+} is of significance to construct hybrid Li-Mg-ion cell by combining $MgMn_2O_4$ with Li_2TiO_3 oxides as electrodes.

Experimental

Monoclinic Li_2TiO_3 was obtained by hydrothermal method using TiO_2 and concentrated LiOH solution, followed by temperature annealing at 400 ^oC. The preparation of $MgMn_2O_4$ spinel relies on the thermal decomposition of mixed magnesium-manganese formate precursors, which are obtained by freeze-drying of corresponding magnesium-manganese formate solution. The precursor decomposition proceeds at 350 ^oC for duration of 3 h. To improve the crystallinity, the oxides were annealed at 550 ^oC for 6 hours.

The structure and morphology of oxides were determined by powder X-ray diffraction, SEM and TEM analysis. The powder X-ray structural analysis was carried out on a Bruker Advance 8 diffractometer with a LynxEye detector (CuKα radiation). All XRD patterns were recorded at 0.02^o 2Θ steps of 2 s duration. The computer program WinPLOTR was used for XRD patterns calculation. The SEM analysis is observed by JEOL JSM 6390 scanning electron microscope equipped with an energy dispersive X-ray spectroscopy (EDS, Oxford INCA Energy 350) and ultrahigh resolution scanning system (ASID-3D) in a regime of secondary electron image (SEI). The TEM investigations were performed on a JEOL 2100 transmission electron microscope and a JEOL 2100 XEDS: Oxford Instruments, X-MAX^N 80T CCD Camera ORIUS 1000, 11 Mp, GATAN at accelerating voltage of 200 kV. The oxide suspensions in acetone were dripped on standard holey carbon/Cu grids. The Digital Micrograph software was used for sample analysis.

The electrochemical performance of oxides was accomplished by using half-ion cells type Swagelok consisting of $Li|LiPF_6(EC:DMC)|MgMn_2O_4$ (or Li_2TiO_3). The electrodes, supported onto an aluminium foil with purity of 99%, were a mixture containing 80% of the active compositions, 5% poly (vinylidene fluoride) (PVDF), 7.5% C-NERGY KS 6 L graphite (TIMCAL) and 7.5% Super C65 (TIMCAL). The loaded mass of active materials on Al collectors was about 2-4 mg. Two types or electrolyte solutions were used: lithium electrolyte consisting of 1 M solution of $LiPF_6$ in ethylene carbonate–dimethyl carbonate (1:1 by volume), and magnesium electrolyte based on 0.5 M $Mg(TFSI)_2$ solution in diglyme. The lithium electrodes consisted of a clean lithium metal disk with diameter of 10 mm. The cells were assembled in a glove box under argon atmosphere. The electrochemical reactions were tested on Arbin BT2000 system with eight-channels in galvanostatic mode. The structural changes in the electrode compositions during electrochemical reaction were monitored on electrodes cycled in lithium and magnesium electrolyte for 10 cycles. The cell is stopped at 1.7 V, then it is disassembled insight a glove box, followed by removal and washing of the working electrodes with EC.

Results and Discussions

The thermal decomposition of mixed magnesium-manganese formate precursor yields at 350 ^oC a tetragonally distorted $MgMn_2O_4$ spinel (s.g. $I4_1/amd$, Fig. 1). The tetragonal structure is preserved after increasing the annealing temperature from 350 to 550 ^oC (Fig. 1). The unit cell parameters for oxides annealed at 350 ^oC and 550 ^oC are a=5.813 Å, c=9.250 Å and a=5.727 Å, c= 9.300 Å, respectively. The ratio between the *c*- and *a*- lattice parameter expresses the extent of tetragonal distortion: $c/(2^{1/2}a)$=1.125 and $c/(2^{1/2}a)$=1.148 for $MgMn_2O_4$ annealed at 350 ^oC and at 550 ^oC, respectively. The structural analysis reveals an increase in the tetragonal distortion of the spinel structure with enhancement of the annealing temperature. This is related with distribution of Jahn-Teller Mn^{3+} and Mg^{2+} ions over two crystallographic spinel positions. The larger tetragonal distortion is achieved when Jahn-Teller Mn^{3+} and Mg^{2+} ions are stabilized on octahedral and tetrahedral spinel sites (oxide known as normal spinel) [17]. This is what we observe for $MgMn_2O_4$ annealed at 550 ^oC. The Mg^{2+} ions are prone to participate in exchange reactions with manganese ions, as a result of which part of Mg^{2+} ions

appears in the octahedral sites concomitant with a corresponding part of manganese ions - in tetrahedral sites (oxide known as inverse spinel) [17]. The cationic redistribution of Mg^{2+} between tetrahedral and octahedral spinel sites leads to a reduction of the tetragonal distortion of the spinel structure. It seems that, at lower annealing temperature (i.e. at 350 ^{o}C), $MgMn_2O_4$ adopts inverse spinel configuration with lower extent of tetragonal distortion. The Mg^{2+} and Mn^{3+} distribution in the oxide structure has been predicted, on the basis of first-principles calculations and percolation theory, to influence the electrochemistry of spinels such as $MgMn_2O_4$ and $MgIn_2S_4$ [18]. In this study, we provide experimental evidence on the effect of the cationic spinel distribution on the mechanism of Li^+ and Mg^{2+} intercalation.

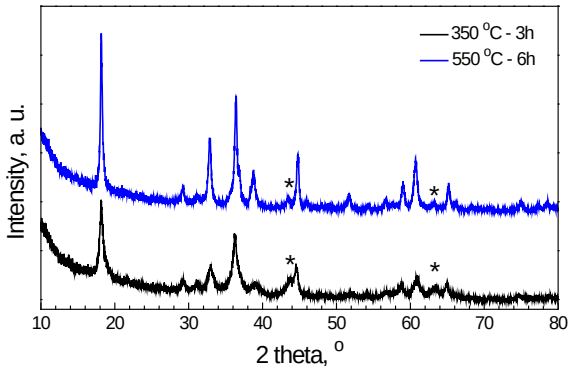

Fig. 1. XRD patterns of $MgMn_2O_4$ annealed at 350 ^{o}C for 3 hours and at 550 ^{o}C for 6 hours. The asterisk denotes the impurity oxide phase with rock-salt structure.

In addition, the XRD patterns become narrower when the annealing temperature increases, thus indicating a growing of the crystallite sizes. To check this suggestion, Figure 2 gives the TEM images of $MgMn_2O_4$ annealed at 350 and 550 ^{o}C. As one can see, $MgMn_2O_4$ displays nanometric particles with sizes varying between 10 and 35 nm. Although both small and big particles can simultaneously be distinguished for the low-temperature annealed spinel, the high-temperature annealed spinel posses well shaped particles with close particle size distribution around 35 nm. It is noticeable that, in the literature, this is a lowest temperature reported for the synthesis of well-crystallized $MgMn_2O_4$ [19].

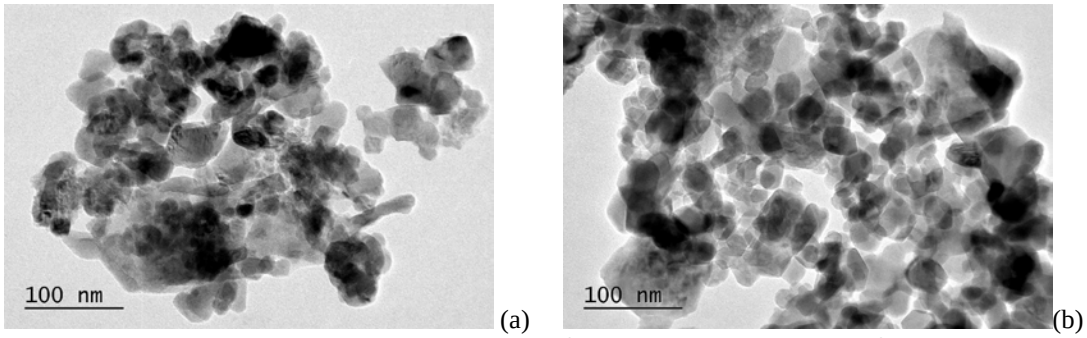

(a) (b)

Fig. 2. TEM images of $MgMn_2O_4$ annealed at 350 ^{o}C for 3 hours (a) and at 550 ^{o}C for 6 hours (b).

Because of the specific cationic distribution and the nanometric particles, $MgMn_2O_4$ is able to intercalate reversibly both Li^+ and Mg^{2+} ions. The intercalations of Li^+ and Mg^{2+} into $MgMn_2O_4$ are compared on Figure 3. The electrochemical intercalation reactions are simply controlled by the composition of the used electrolyte: $LiPF_6$- and $Mg(TFSI)_2$-based electrolytes, respectively. The stable electrochemical response is obtained after few initial cycles. In lithium electrolyte, lithium intercalation into $MgMn_2O_4$ is accomplished between 1.8 and 4.4 V by delivering a reversible capacity of about 95 mAh/g. It is of importance that charge and discharge curves display smooth changes during Li mobility into inverse spinel $MgMn_2O_4$ (i.e. annealed at 350 ^{o}C). For sake of comparison, the normal spinel oxide $MgMn_2O_4$ (i.e. annealed at 550 ^{o}C) exhibits two well-resolved plateaus where Li intercalation takes place: low-voltage plateau at 3.05/2.80 V and high voltage-plateau at 4.05/3.85 V, respectively. The two plateaus are typical for the lithium intercalation into $LiMn_2O_4$ spinel. This means that the normal spinel $MgMn_2O_4$ is transformed into $LiMn_2O_4$ during Li^+ intercalation. It is worth mentioning that $LiMn_2O_4$ is classified also as a normal spinel since Li^+ and $Mn^{3+/4+}$ ions occupy tetrahedral and octahedral sites, respectively. The formation of tetragonal $MgMn_2O_4$ and cubic $LiMn_2O_4$ from λ-MnO_2 has recently been demonstrated when the electrochemical reaction is performed in aqueous solutions [19]. Contrary to normal

spinel, it appears that the inverse spinel $MgMn_2O_4$ is not converted into $LiMn_2O_4$ spinel during cycling (Fig. 3). In addition, inverse spinel $MgMn_2O_4$ exhibits higher reversible capacity than that of normal spinel $MgMn_2O_4$. The stability of both normal and inverse spinels $MgMn_2O_4$ and their high reversible capacity suggests that the electrochemical reaction includes both Li^+ and Mg^{2+} intercalation.

The dual intercalation of Li^+ and Mg^{2+} into $MgMn_2O_4$ is further examined by the experiment, where the $LiPF_6$-based electrolyte is replaced with $Mg(TFSI)_2$-based electrolyte (Fig. 3). As one can see, the charge discharge curves undergo some changes in respect of their profiles. The comparison shows that charge and discharge curves become smoother concomitantly with increasing the irreversibility of the intercalation reaction especially in the few first cycles (Fig. 3): the irreversible capacity is about 30 mAh/g. The higher irreversibility of Mg^{2+} intercalation is related with kinetic limitations. However, the first charge capacity in $Mg(TFSI)_2$-electrolyte is close to that in $LiPF_6$-electrolyte: 92 versus 98 mAh/g, respectively. During further cycling, the irreversibility is reduced and Coulombic efficiency become higher than 97 %. It is of importance that the discharge capacity in the magnesium electrolyte is still higher: 50 – 55 mAh/g. All these results give evidence for complex intercalation reactions of Li^+ and Mg^{2+} into inverse $MgMn_2O_4$, which depend on the kind of the cationic distribution in spinel structure, as well as on the composition of used electrolyte.

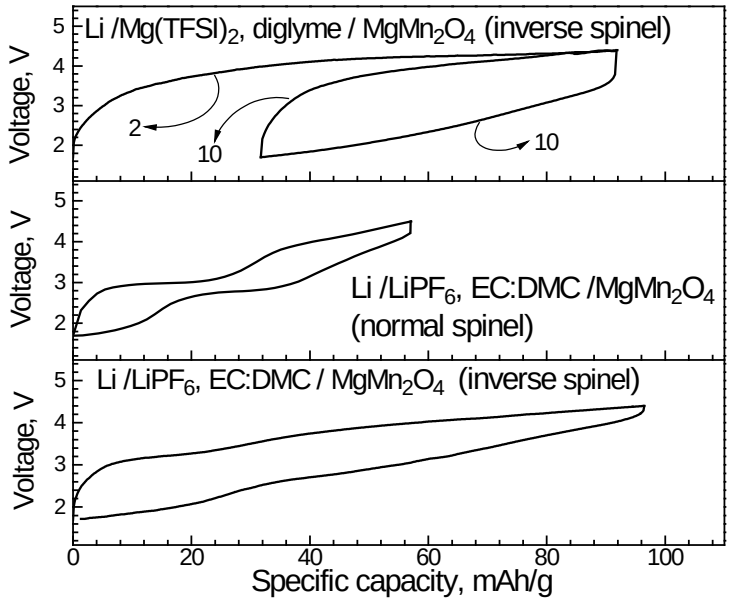

Fig.3. Charge discharge curves of $MgMn_2O_4$ in $LiPF_6$- and $Mg(TFSI)_2$-based electrolytes after 10 cycles. For sake of convenience, the charge curve of 2 cycle for inverse MgMn2O4 in $Mg(TFSI)_2$-based electrolyte is also shown.

To understand the mechanism of metal ion intercalation into normal and inverse spinels, *ex-situ* HR-TEM analysis is undertaken. Figure 4 compares the bright field TEM images of normal and inverse spinel cycling in lithium and magnesium electrolyte. The nanometric particles and particle distribution for inverse and normal spinels remain intact after the electrochemical reaction irrespective of the composition of the used electrolyte. HR-TEM images of selected particles show an appearance of closely interconnected nanodomains with different extent of tetragonal distortion. The calculations along [111] and [010] directions permit to distinguish nanodomains with at least three different extent of tetragonal distortion: (i) nanodomains with a distortion close to that of the pristine spinel are observed for inverse $MgMn_2O_4$ cycled in lithium and magnesium electrolytes; (ii) nanodomains with a distortion higher than the pristine composition (i.e. $c/(2^{1/2}.a)$=1.17) are visible for both inverse and normal spinels cycled in lithium electrolyte, and (iii) nanodomains with a distortion lower than the pristine composition (i.e. $c/(2^{1/2}.a)$=1.08) appear only for inverse spinel cycled in magnesium electrolyte. To rationalize the observed variation in the extent of tetragonal distortion, one can take into account the possible phases containing magnesium and lithium, which crystallize in tetragonally distorted spinel structure. The well-known lithium intercalated spinel $Li_2Mn_2O_4$ is tetragonally distorted and the "$c/(2^{1/2}.a)$"-ratio reaches a value of 1.17. This value is close to that observed by us for inverse and normal spinels cycled in lithium electrolyte, which allows to associate nanodomains with a phase having a higher amount of lithium (i.e. Li_2MnO_4-like phase). The formation of $Li_2Mn_2O_4$-like phase due to preferential Li^+ intercalation is in agreement with two voltage plateaus observed in charge/discharge curves of normal $MgMn_2O_4$ cycled in lithium electrolyte (Fig. 3). The differences in the electrochemical behavior of inverse and normal spinel are also supported by nanodomain structure observed by *ex-situ* TEM analysis. In the case of the inverse spinel, the slightly lower distortion of

nanodomains indicates some differences in $Li_2Mn_2O_4$-phase composition, which in its turn is manifested by the lack of plateaus in the charge/discharge curves (Fig. 3). This can be understood if we suppose that co-intercalation of Mg^{2+} and Li^+ ions takes place at inverse spinel cycled in lithium electrolyte.

Furthermore, the extent of the tetragonal distortion is reduced by decreasing the amount of Mg in Mg-containing manganates, $Mg_xMn_{2-x}O_4$ with x<1 [17]. Therefore, the nanodomains with lower extent of tetragonal distortion originate from spinels with decreased Mg-to-Mn ratio (i.e. Mg/Mn<0.5). To support these observations, the chemical composition of cycled spinels is evaluated by BF-STEM. The results show that the Mg-to-Mn ratio decreases after cycling, this decrease is more significant for inverse spinel cycled in $Mg(TFSI)_2$-electrolyte: Mg/Mg=0.50 for pristine spinel and Mg/Mn=0.45 for inverse spinel cycled in lithium electrolyte, Mg=0.36 for normal spinel cycled in lithium electrolyte and Mg/Mn=0.11 for inverse spinel cycled in magnesium electrolyte. The observation of Mg-poor spinel during electrochemical cycling of the inverse spinel in magnesium electrolyte implies for proceeding of preferential Mg^{2+} intercalation instead of Li^+ one. This is the opposite to the electrochemical behavior of the inverse spinel in lithium electrolyte, where Li^+ intercalation prevails.

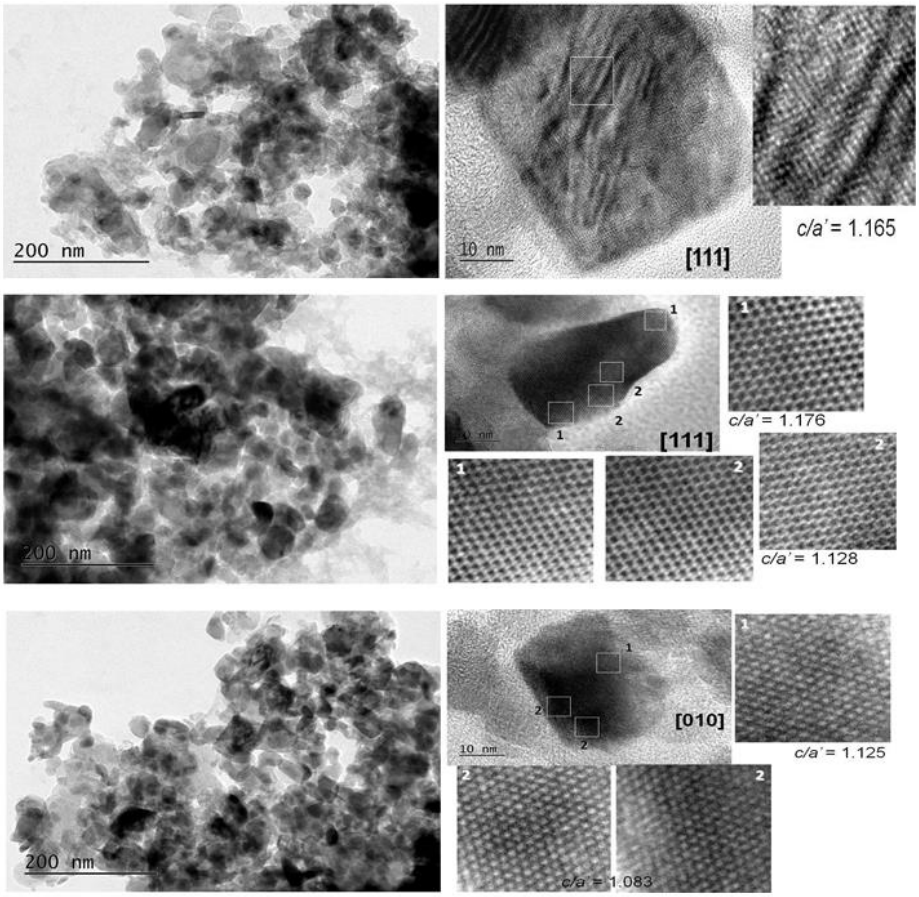

Fig. 4. Bright field micrographs and HR-TEM images for inverse $MgMn_2O_4$ cycled in lithium electrolyte (top), normal $MgMn_2O_4$ cycled in lithium electrolyte (middle) and inverse $MgMn_2O_4$ cycled in magnesium electrolyte (bottom). The calculated extent of tetragonal distortion ($c/a'=c/(2^{1/2}.a)$) is also denoted.

In comparison with $MgMn_2O_4$, the well-known $Li_4Ti_5O_{12}$ spinel displays non-selective intercalation properties in respect of Li^+ and Mg^{2+} ions [20]: a flat voltage plateau of 1.55 V *versus* Li/Li^+ is a specific feature for Li^+ intercalation into $Li_4Ti_5O_{12}$, while Mg^{2+} intercalation is accomplished in the range of 1.7-0.7 V *versus* Mg/Mg^{2+}, respectively [20]. The intercalation mechanism is also different [20]. $Li_4Ti_5O_{12}$ accommodates Li^+ ions thanks to the reversible two-phase reaction between spinel and rocksalt structure: $Li_4Ti_5O_{12} + 3Li^+ \leftrightarrow Li_7Ti_5O_{12}$. The phase transformation and separation is also established during Mg^{2+} intercalation into $Li_4Ti_5O_{12}$, the mechanism being more complex following the chemical equation: $2Li_4Ti_5O_{12} + 3Mg^{2+} \rightarrow Li_7Ti_5O_{12} + Mg_4LiTi_5O_{12} \rightarrow Mg_{2.5}LiTi_5O_{12} \leftrightarrow Mg_4LiTi_5O_{12}$ [20]. Taking into account the above findings, in this study we demonstrate that monoclinic Li_2TiO_3 is also able to intercalate Li^+ and Mg^{2+} ions. This is a consequence of both the structure and morphology of Li_2TiO_3 (Fig. 5). Li_2TiO_3 adopts a monoclinic structure in accordance with

previously reported data [21]. The morphology consists of micrometric aggregates (3 – 30 μm), which are composed of closely bounded primary particles (Fig. 5).

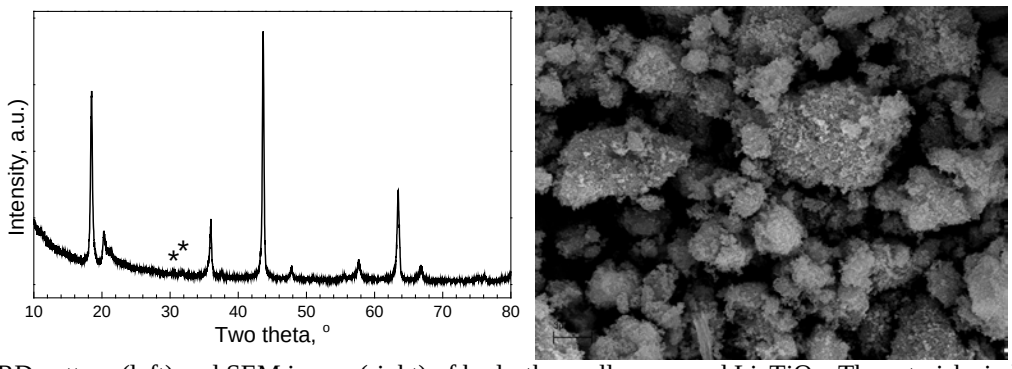

Fig. 5. XRD pattern (left) and SEM image (right) of hydrothermally prepared Li_2TiO_3. The asterisks indicate the impurity of Li_2CO_3.

Figure 6 compares the charge/discharge curves of monoclinic Li_2TiO_3 and spinel $Li_4Ti_5O_{12}$ cycled in half-ion cells versus metallic lithium in lithium and magnesium electrolytes. As one can expect, in lithium electrolyte $Li_4Ti_5O_{12}$ spinel intercalates Li^+ at 1.57/1.54 V by delivering a reversible capacity of 150 mAh/g. When lithium electrolyte is replaced by magnesium one, the reversible capacity remains intact. However, the potential of Li^+ intercalation undergoes some changes during cycling: the oxidation and reduction voltage tend one to another and after 5 cycles they reaches 1.60 V and 1.50 V, respectively. Contrary to $Li_4Ti_5O_{12}$ spinel, the electrochemical performance of monoclinic Li_2TiO_3 displays a strong dependence on the electrolyte composition. In lithium electrolyte, the charge/discharge curves are smooth and the reversible capacity is extremely low (around 18 mAh/g). This reveals that monoclinic Li_2TiO_3 is non-active in comparison with $Li_4Ti_5O_{12}$. The lack of the electrochemically activity for monoclinic Li_2TiO_3 has already been reported [22,23]. When lithium electrolyte is replaced with magnesium one, a drastic improvement in the electrochemical activity of monoclinic Li_2TiO_3 becomes visible: the reversible capacity is about 30-35 mAh/g and charge/discharge curves display small plateau, which is well distinguished after 20 cycles (i.e. the oxidation and reduction potentials are 1.60 and 1.48 V, respectively). It is important that this plateau brings a resemblance with that observed in lithium electrolyte. The enhancement of the reversible capacity in magnesium electrolyte suggests that monoclinic Li_2TiO_3 is able to co-intercalate Mg^{2+} and Li^+ ions. This is the first electrochemical evidence for Mg^{2+}-induced improvement of the Li^+ intercalation, which on its turns allows to convert the inactive Li_2TiO_3 phase into active intercalation matrices.

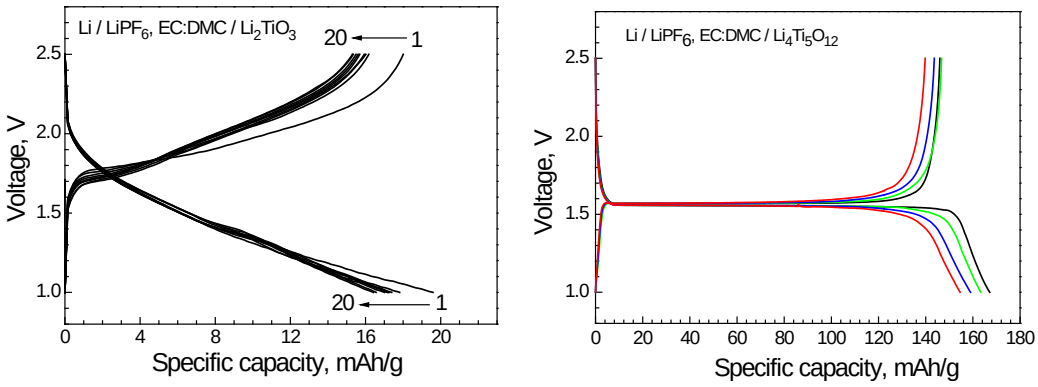

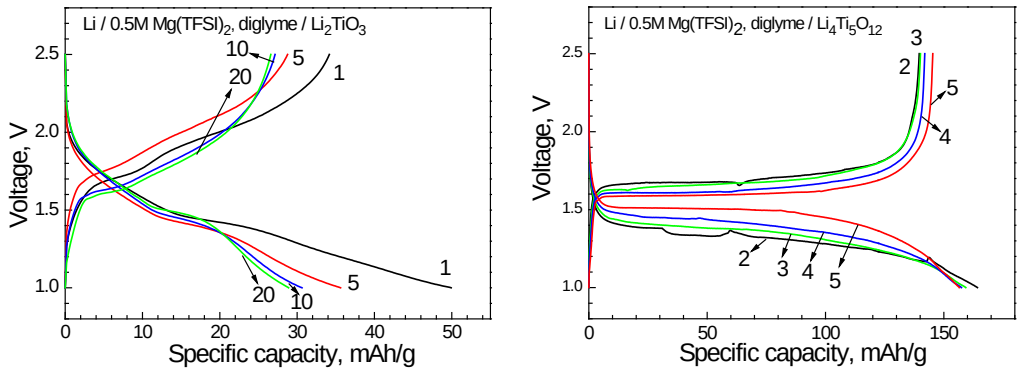

Fig. 6. Charge/discharge curves for monoclinic Li_2TiO_3 (left) and $Li_4Ti_5O_{12}$ spinel (right) cycled in lithium and magnesium electrolytes. The number of cycles is indicated below each curve.

Conclusions

The magnesium-manganese formate precursors yield, at 350 ^oC and short heating time, an inverse $MgMn_2O_4$ spinel having well crystallize particles with sizes between 10 and 35 nm. By increasing the annealing temperature, there is a transformation from inverse to a normal spinel configuration $MgMn_2O_4$, the particle size distribution becomes more narrow. The specific cationic distribution and the nanometric particles contribute to the capability of $MgMn_2O_4$ to intercalate reversibly both Li^+ and Mg^{2+} ions. In lithium electrolyte, the normal spinel $MgMn_2O_4$ intercalates at two plateaus Li^+ preferentially leading to a formation of nanodomains with $Li_2Mn_2O_4$-like phase. Contrary to normal spinel, the inverse spinel $MgMn_2O_4$ displays a co-intercalation of Li^+ and Mg^{2+} ions, as a result of which nanodomains with mixed $Mg_xLi_{2-x}Mn_2O_4$ composition and with a lower tetragonal distortion are developed. This contributes to the enhancement of the reversible capacity delivered by the inverse spinel $MgMn_2O_4$ in comparison with that for the normal spinel configuration: 90-100 mAh/g versus 50-60 mAh/g, respectively. In magnesium electrolyte, the Mg^{2+}-intercalation prevails over Li^+ ones and the resulting reversible capacity for inverse spinel decreases.

The co-intercalation of Li^+ and Mg^{2+} ions is also takes place at monoclinic Li_2TiO_3, which is a driving force to transform non-active intercalataion oxide into suitable structural matrix. As far as we known, this is a first experimental evidence for electrochemical activity of monoclinic Li_2TiO_3 in rechargeable batteries.

In general, the high-efficient energy storage into nanometric spinel $MgMn_2O_4$ and monoclinic Li_2TiO_3 is achieved due to their co-intercalation properties. The proposed approach for improvement of the kinetic of Mg^{2+} intercalation can be extended towards other combination of intercalating ions such as two monovalent alkaline ions or mono- and bivalent ions with different ionic radii. The results of this study are of significance in order to introduce cheaper and safety post-lithium ion batteries.

Acknowledgements: The authors are grateful to the financial support from the National Science Fund of Bulgaria, Project DN09/13.

References

1. Muldoon, J., Bucur, B., Gregory, T.: Quest for nonaqueous multivalent secondary batteries: magnesium and beyond. Chem. Rev. 114, 11683-11720 (2014).

2. Huie, M., Bock, D., Takeuchi, E., Marschilok, M., Takeuchi, K.: Cathode materials for magnesium and magnesium-ion based batteries. Coordination Chemistry Reviews 287, 15–27 (2015).

3. Novak, P., Imhof, R., Haas, O.: Magnesium insertion electrodes for rechargeable nonaqueous batteries — a competitive alternative to lithium?. Electrochim. Acta, 45 (1999) 351–367.

4. Lu Z., Schechter A., Moshkovich M., Aurbach D.: On the electrochemical behavior of magnesium electrodes in polar aprotic electrolyte solutions. J. Electroanal. Chem. 466, 203–217 (1999).

5. Levi, E., Mitelman, A., Aurbach, D., Brunelli, M.: Structural Mechanism of the Phase Transitions in the Mg−Cu−Mo6S8 System Probed by ex Situ Synchrotron X-ray Diffractio. Chem. Mater. 19, 5131–5142 (2007).

6. R. Zhang, X. Yu, K. Nam, C. Ling, T.S. Arthur, W. Song, A.M. Knapp, S.N. Ehrlich, . Yang, M. Matsui, Electrochem. Commun. 23 (2012) 110-113.

7. Sun, X., Bonnick, P., Nazar, L.: Layered TiS_2 Positive Electrode for Mg Batteries, ACS Energy Lett. 1, 297-301 (2016).

8. Sun, X., Bonnick, P., Duffort, V., Liu, L., Rong, Z., Persson, K., Ceder, G., Nazar, L.: A high capacity thiospinel cathode for Mg Batteries. Energy Environ. Sci., 9, 2273-2277 (2016).

9. Gershinsky, G., Yoo, H., Gofer, Y., Aurbach, D.: Electrochemical and spectroscopic analysis of Mg^{2+} intercalation into thin film electrodes of layered oxides: V_2O_5 and MoO_3. Langmuir 29, 10964-10972 (2013).

10. Sutto, T, Duncan, T.: Electrochemical and structural characterization of Mg ion intercalation into RuO2 using an ionic liquid electrolyte. Electrochim. Acta 79, 170-174 (2012).

11. Kaveevivitchai, W., Jacobson, A: High Capacity Rechargeable Magnesium-Ion Batteries Based on a Microporous Molybdenum–Vanadium Oxide Cathode. Chem. Mater. 28, 4593-4601 (2016).

12. Lipson, A., Han, S.-D., Kim, S., Pan, B., Sa, N., Liao, C., Fister, T., Burrell, A., Vaughey, J., Ingram, B.: Nickel hexacyanoferrate, a versatile intercalation host for divalent ions from nonaqueous electrolytes. J. Power Sources 325, 646-652 (2016).

13. Mizuno, Y., Okubo, M., Hosono, E., Kudo, T., Oh-Ishi, K., Okazawa, A., Kojima, N., Kurono, R., Nishimura, S.-I., Yamada, A.: Electrochemical Mg^{2+} intercalation into a bimetallic CuFe Prussian blue analog in aqueous electrolytes. J. Mater. Chem. A 1, 13055-13059 (2013).

14. Ling, C., Banerjee, D., Song, W., Zhang, M., Matsui, M.: First-principles study of the magnesiation of olivines: redox reaction mechanism, electrochemical and thermodynamic properties, J. Mat. Chem. 22, 13517-13523 (2012).

15. Chen, X., Bleken, F., Løvvik, O., Vullum-Bruer, F.: Comparing electrochemical performance of transition metal silicate cathodes and chevrel phase Mo6S8 in the analogous rechargeable Mg-ion battery system, J. Power Sources 321, 76-86 (2016).

16. Chae, M., Hyoung, J., Jang, M., Lee, L., Hong, S.-T.: Potassium nickel hexacyanoferrate as a high-voltage cathode material for nonaqueous magnesium-ion batteries, Journal of Power Sources 363, 269-276 (2017).

17. Malavasi L., Ghigna, P., Chiodelli, G., Maggi, G., Flor, G.: Structural and Transport Properties of $Mg_{1-x}Mn_xMn_2O_{4\pm\delta}$ Spinels. J. Solid State Chem. 166, 171-176 (2001).

18. Gautam, G., Canepa, P., Urban, A., Bo, S.-H., Ceder, G.: Influence of Inversion on Mg Mobility and Electrochemistry in Spinels. Chem. Mater. 29, 7918−7930 (2017).

19. Cabello, M., Alcantara, R., Nacimiento, F., Ortiz, F., Lavela, P., Tirado, J.: Electrochemical and chemical insertion/deinsertion of magnesium in spinel-type $MgMn_2O_4$ and lambda-MnO_2 for both aqueous and non-aqueous magnesium-ion batteries. CrystEngComm 17, 8728-8735 (2015).

20. Wu, N., Lyu, Y.-C., Xiao, R.-J., Yu, X., Yin, Y.-X., Yang, X.-Q., Li, H., Gu, L., Guo, Y.-G.: A highly reversible, low-strain Mg-ion insertion anode material for rechargeable Mg-ion batteries, NPG Asia Materials volume6, pagee120 (2014)NPG Asia Materials 6, 120-126 (2014).

21. Yu, C.-L., Yanagisawa, K., Kamiya, S., Kozawa, T., Ueda, T.: Monoclinic Li_2TiO_3 nano-particles via hydrothermal reaction: Processing and structure. Ceramics International 40, 1901-1908 (2014).

22. Wang, Y., Zhou, A., Dai, X., Feng, L., Li, J.: Solid-state synthesis of submicron-sized $Li_4Ti_5O_{12}/Li_2TiO_3$ composites with rich grain boundaries for lithium ion batteries, J. Power Sources 266, 114-120 (2014).

23. Tabuchi, M., Nakashima, A., Shigemura, H., Ado, K., Kobayashi, H., Sakaebe, H., Tatsumi, K., Kageyama, H., Nakamura, T., Kanno, R.: Fine $Li_{(4-x)/3}Ti_{(2-2x)/3}Fe_xO_2$ ($0.18 \leq x \leq 0.67$) powder with cubic rock-salt structure as a positive electrode material for rechargeable lithium batteries. J. Mater. Chem. 13, 1747-1757 (2003).